For submission to: Chemosphere

Title: Impact of Microbial Iron Oxide Reduction on the Transport of Diffusible Tracers and Non-diffusible Nanoparticles in Soils

Authors: Xiaolong Liang[a], Mark Radosevich[a], Frank Löffler[a,b,c], Sean M. Schaeffer[a], and Jie Zhuang[a,*]

Addresses:

[a]Department of Biosystems Engineering and Soil Science, The University of Tennessee, Knoxville, TN 37996, USA

[b]Department of Microbiology, Department of Civil and Environmental Engineering, Center for Environmental Biotechnology, The University of Tennessee, Knoxville, TN 37996, USA

[c]Biosciences Division, Oak Ridge National Laboratory, Oak Ridge, TN 37831, USA

Address correspondence to Jie Zhuang: jzhuang@utk.edu

Key words: Biostimulation, iron reduction, nanoparticles, transport, soil aggregates

Highlights

- Fe(III)-bioreduction causes time-dependent aggregate breakdown and colloid release.
- Short-term bioreduction alters soil aggregate surface chemistry and tracer transport.
- Electron donor amendment enhances transport of nanoparticle tracer.

Abstract

In situ bioremediation to achieve immobilization of toxic metals and radionuclides or detoxification of chlorinated solvents relies on electron donor additions. This practice promotes microbial Fe(III)-oxide mineral reduction that could change soil pore structure, release soil colloids, alter matrix surface properties, and cause the formation of secondary (i.e., reduced) Fe-mineral phases. These processes in turn may impact rates of bioremediation, groundwater quality, and ultimately contaminant fate. Continuous flow columns packed with water-stable soil aggregates high in Fe-oxides were infused with artificial groundwater containing acetate as electron donor and operated for 20 or 60 days inside an anoxic chamber. Soluble Fe(II) and soil colloids were detected in the effluent within one week after initiation of the acetate addition, demonstrating Fe(III)-bioreduction and colloid formation. Br^-, 2,6-difluorobenzoate (DFBA), and silica-shelled silver nanoparticles (SSSNP) were selected as diffusible tracer, low-diffusible tracer, and non-diffusible nanoparticles, respectively, to perform transport experiments before and after the active 20-day bioreduction phase, with an aim of assessing the changes in soil structure and surface chemical properties resulting from Fe(III)-bioreduction. The transport of diffusible Br^- was not influenced by the Fe(III)-bioreduction as evidenced by identical breakthrough curves before and after the introduction of acetate. Low-diffusible DFBA showed earlier breakthrough and less tailing after the bioreduction, suggesting alterations in flow paths and surface chemical properties of the soils. Similarly, non-diffusible SSSNP exhibited early breakthrough and enhanced transport after the bioreduction phase. Unexpectedly, the bioreduction caused complete retention of SSSNP in the soil columns when the acetate injection was extended from 20 days to 60 days, though no changes were observed for Br^- and DFBA during the extended bioreduction period. The large change in the transport of SSSNP was attributed to the enhancement of soil aggregate breakdown and soil colloid release causing

25 mechanical straining of SSSNP and the exposure of iron oxide surfaces previously unavailable
26 within aggregate interiors favorable to the attachment of SSSNP. These results demonstrate that
27 microbial activity can affect soil properties and transport behaviors of diffusivity-varying solutes
28 and colloids in a time dependent fashion, a finding with implication for interpreting the data
29 generated from soil column experiments under continuous flow.
30

1. Introduction

Subsurface bioremediation brought about by electron donor addition creates anoxic conditions that stimulate the growth of iron reducing and/or sulfate reducing bacteria (Chapelle and Lovley, 1992; Si et al., 2015). Subsequently, oxidized forms of iron are reduced to Fe(II), solubilizing iron oxide minerals. The soluble Fe(II) and secondary precipitation of iron (e.g., ferrous hydroxide) can result in abiotic transformation of contaminants and/or the release of colloidal clay and iron mineral colloids (Pedersen et al., 2006; Thompson et al., 2006). Adsorption of contaminants to these colloids may enhance contaminant transport via colloid-facilitated transport (Bose and Sharma, 2002; Zhuang et al., 2003). Additionally, biomass increase and colloid production can cause pore clogging, potentially reducing hydraulic conductivity of the porous medium down gradient from the treatment zone. Alternatively, advective flow paths and increased hydraulic conductivity may trigger substantial soil aggregate breakdown. Thus, altering the indigenous properties of subsurface media may impact coupled processes controlling the fate and transport of contaminants, and cause unintended secondary impacts on the properties of the porous media and groundwater quality (e.g. secondary mineral precipitates, permeability, and microbial activity).

Anaerobic bioremediation is an attractive technology for subsurface soil and water remediation based on cost and effectiveness (Ellis et al., 2000; Coates and Anderson, 2000; Liang et al., 2017). The technology generally aims to create anoxic conditions via addition of soluble electron donors, such as acetate and lactate or higher molecular weight substrates, for stimulating microorganisms that degrade organic contaminants (e.g. chlorinated solvents) and reduce heavy metals and radionuclides to insoluble forms thereby immobilizing them *in situ* (Aulenta et al., 2006). Once anoxic conditions are achieved, anaerobic respiration with available

54 electron acceptors is stimulated leading to biologically-mediated reduction of Fe(III)-oxide
55 minerals (the most common mineral oxide of soils and subsurface environments) and the
56 formation of soluble Fe(II) (Caldwell et al., 1999; Weber et al., 2006; Mejia et al., 2016). Iron
57 oxides, which have diverse crystallinities and reactivity (e.g. ferrihydrite, goethite, lepidocrocite,
58 and hematite), are extensively present in soils (Pedersen et al., 2006; Vink et al., 2017). The
59 indigenous iron oxides serve a very important role as aggregating agents that "cement" clay
60 particles together into aggregates (Goldberg et al., 1990; Braunschweig et al., 2013). Reduction
61 of Fe(III)-oxides under anoxic conditions may cause disintegration of soil aggregates and
62 generate mobile colloids (Hansel et al., 2005; De-Campos et al., 2009). These processes may
63 disrupt pore structure and alter pore connectivity, flow paths, and permeability (Guan et al.,
64 2017). These alterations could either promote or inhibit the transport of solutes and colloids.
65 Schaider et al. (2014) found that iron oxide aggregates can alter the transport of particulate
66 particles and sequester metals. The formation and mobilization of colloids can act as vectors to
67 facilitate co-transport of solutes and toxic metals in soils and groundwater (McCarthy and
68 McKay, 2004; Maurice and Hocella, 2008; Guan et al., 2017). The reduction of Fe(III)-oxides
69 may also change soil surface properties to influence the reactive transport processes (Hansel et
70 al., 2003; Jardine, 2008).

71 Transport of solutes and colloids in soil is influenced by the pore structure and surface
72 chemistry of soils, solution chemistry, and hydrological conditions (Zhuang et al., 2005; 2007;
73 2010; Bradford and Torkzaban, 2008; Mohanty et al., 2016; Pachapur et al., 2016). The
74 influencing mechanisms have been well examined at varying scales from laboratory columns
75 (repacked or undisturbed) to field scale (McKay et al., 2000; Arora et al., 2015; Karadimitriou et
76 al., 2017). Bioremediation treatment may alter aquifer porosity, flow paths, and mineral

77 interfacial properties and in turn change the attenuation and migration of solutes, colloids, and
78 microbial cells; all these may exert feedback effects on microbial bioremediation.
79 Microorganisms, nutrients, or electron donors are generally applied to accelerate in situ
80 bioremediation (Ellis et al., 2000; Lovley 2003; Moon et al., 2017), yet the remediation
81 efficiency is subject to their mobility in porous media (Song et al., 2017). Thus far, few studies
82 have addressed the impacts of biostimulation on the transport of solutes and colloids, making
83 difficult to resolve the low-efficiency problem of bioremediation under field conditions.
84 Therefore, in-depth investigations are needed to understand the potential that biostimulation
85 influences the mobility of solutes and colloids including microorganisms.

86 The objective of this research was to assess the impact of biologically-mediated Fe(III)-
87 oxide reduction on the transport of solutes and colloids with respect to soil structure breakdown
88 under saturated flow conditions, shedding light on the interplays of microbial activities with the
89 solutes and colloids migration during bioremediation processes. Breakthrough tests with
90 diffusivity-varying tracers and non-diffusing nanoparticles both before and after acetate-
91 stimulated Fe(III)-bioreduction were conducted to evaluate the alteration of soil surface
92 chemistry and flow pathways. The research provides significant insights into the feedback effects
93 of anoxic bioremediation on the transport of solutes and colloids, microbial distribution, and soil
94 aggregate structure.

95 **2. Materials and methods**

96 *2.1 Porous media*

97 The columns were packed with different porous media, including uncoated and goethite-
98 coated silica sand and water-stable soil aggregates extracted from an iron oxide-rich natural soil.

99 The sand grains had a median diameter (d_{50}) of 0.25 ± 0.01 mm with a trade name Accusand
100 (Grade 50/70, Unimin Corporation, New Canaan, CT, USA). Prior to coating with goethite, the
101 sand was chemically treated to remove natural metal oxides from the grains following the
102 established procedure (Zhuang and Jin, 2003). Goethite synthesis and coating on the cleaned
103 sand were performed as described by Zhuang and Jin (2008). The natural soil was collected from
104 an eroded agricultural site mapped as the Decatur silty clay loam. The Decatur series is a fine,
105 kaolinitic, thermic rhodic Paleudults. Soil aggregates were extracted by wet sieving of the bulk
106 soils through 2,000, 250, and 53 μm sieves using the modified method as described in Zhuang et
107 al. (2008). Two fractions of water-stable soil aggregates, microaggregates (53-250 μm) and
108 macroaggregates (250-2000 μm), were obtained and then air-dried for experimental use. The
109 citrate-bicarbonate-dithionite extractable iron (Mehra and Jackson, 1960) of the bulk soil,
110 microaggregates, and macroaggregates were 5.5%, 4.7% and 5.2% (w/w), respectively, as
111 measured using the ferrozine method (Viollier et al., 2000).

112 *2.2 Tracers and nanoparticles*

113 Two diffusible tracers and one non-diffusing nanoparticle were used for transport
114 experiments, including bromide (Br^- in KBr) (ionic diffusible tracer), 2,6-difluorobenzoate
115 (DFBA) (molecular diffusible tracer with lower diffusivity than Br^-) (Mayes et al., 2003), and
116 silica-shelled silver nanoparticles (SSSNP) (non-diffusible particle). The SSSNP was purchased
117 from nanoComposix (http://nanocomposix.com/) and has a core of silver nanoparticles with
118 average diameter of 106 nm. The silver cores are encased in a shell of silica with average
119 thickness of 22 nm, resulting in a total particle diameter of 150 nm. The SSSNP were negatively
120 charged, with a measured zeta potential of -5.7 mV at pH 8. SSSNP were specifically selected as
121 a "non-diffusing" particle and potentially as a non-reactive particle given the silica shell

surrounding the silver-core. Advantages to using these shelled particles instead of other previously used particle tracers, such as viruses (e.g., MS-2), are their resistance to biotic and abiotic breakdown, the ease and accuracy of quantification in the effluent samples using graphite furnace atomic absorption spectroscopy, and the convenience to distinguish introduced SSSNP from native soil colloids for mechanistic understanding of transport processes.

2.3 Bacterial strain, growth media, and inoculation for stimulated bioreduction

Geobacter species, with capacity to oxidize organic compounds coupled with reduction of iron oxides or other metal minerals, are ubiquitous in subsurface environments (Caccavo et al., 1994). As such, *Geobacter,* and other microorganisms with similar metabolism have been extensively studied and used for anaerobic bioremediation (Lovley 2003; Moon et al., 2017). To ensure active Fe(III) bioreduction, the soil macroaggregates (250-2,000 μm) were inoculated with laboratory-grown culture of *Geobacter sulfurreducens* strain PCA (ATCC 51573; Caccavo et al., 1994) prior to packing the columns.

Specifically, *G. sulfurreducens* was grown in mineral salts medium containing 1.0 g of NaCl, 0.5 g of $MgCl_2$, 0.2 g of KH_2PO_4, 0.3 g of NH_4Cl, 0.3 g of KCl, 0.015 g of $CaCl_2$, 1 mg of resazurin, and 2 ml of trace element solution, amended with 5 mM acetate and 10 mM ferric citrate per liter was prepared as described by Löffler et al. (1996). The prepared medium was boiled and transferred to serum bottles while flushing with oxygen-free 80/20 (v/v) N_2-CO_2, and the pH was adjusted to 7.2 with flow of CO_2. The serum bottles were autoclaved, and filter-sterilized (with a 0.22 μm Millex filter syringe) acetate and ferric citrate were added to the medium to a final concentration of with 5 mM and 10 mM, separately. The serum bottles inoculated with *G. sulfurreducens* were cultured at 30 °C (Löffler et al., 1996). Once the cultures

144 reached stationary phase (3-5 d; optical density at 600 nm = 0.2 to 0.35; cell concentration of
145 approximately 1×10^8 cells per milliliter), 200 ml of culture suspension was centrifuged at 4,248
146 g, and the bacterial pellet was resuspended in 15 ml of the growth medium in the anaerobic
147 chamber with an 80/20 (v/v) N_2/CO_2 atmosphere. Then, all the resuspended *G. sulfureducens*
148 were uniformly sprayed onto 600 g of air-dried but non-sterile, water-stable soil
149 macroaggregates that were thinly spread on a tray inside the anaerobic chamber. During the
150 application of cell suspension, the aggregates were continuously mixed using a glass rod to
151 achieve uniform inoculation of the bacteria.

152 *2.4 Transport experiment*

153 All transport experiments were conducted in plexiglass (acrylic) columns (25 cm in length
154 with an inside diameter of 3.8 cm) with input solution introduced from the bottom of the column
155 in pulse input mode through a peristaltic pump at pore velocity of 24.4 cm/h. Teflon tubing was
156 used throughout the system except for a portion of tygon tubing needed in the pump. The
157 columns were fitted with five ports connected to pressure sensors (Honeywell Sensing and
158 Control, Inc., USA), which were separated by 5-cm intervals along the column length. Real-time
159 data of hydrostatic pressure were collected with data loggers of CR-1000 Measurement and
160 Control Systems (Campbell Scientific, Inc., Logan Utah) to calculate hydraulic conductivity
161 between different sections of the columns according to the difference in pressure. During the
162 transport experiment, liquid effluent was collected from the top of the column into 20-mL glass
163 tubes using Retriever II fraction collectors for determining the concentrations of tracers, iron,
164 and or colloids as described in section 2.5. The protocols for column experiments are shown in
165 supplementary materials (Table S1 and Fig. S1).

166 Three sets of separate transport experiments were conducted using vertical columns under
167 saturated steady-state flow conditions. The first set aimed to evaluate the appropriateness of use
168 of SSSNP as non-diffusible particle tracer and the effect of iron oxide on the transport of tracers
169 and nanoparticles. The experiments included two columns that were wet-packed with uncoated
170 and goethite-coated sands, respectively. The sand columns were flushed with KCl solution (0.67
171 mM, pH 6.5) prior to the tracer experiments. The input solution for the sand columns contained
172 Br^- (50 mg L^{-1} KBr), DFBA (40 mg/L), and SSSNP (40 ug L^{-1}) in the KCl solution.

173 The second set of experiments aimed to evaluate the effect of Fe(III)-bioreduction on the
174 transport of tracers using five columns dry-packed with *Geobactor*-inoculated soil
175 macroaggregates under anoxic conditions. The experiments included three acetate-stimulated
176 Fe(III)-bioreduction columns (one with 20 days of continuous injection of acetate and two
177 replicates with 60 days of acetate injection) and two control columns (no acetate addition). The
178 60-day experiments aimed to corroborate the results of bioreduction effects observed from the
179 20-day experiments. After dry packing, the soil aggregate columns were flushed with carbon
180 dioxide to replace the air in soil pores, followed by flushing with KCl solution (0.67 mM, pH
181 6.5) to achieve fully saturated conditions without remaining gas pockets. Each column
182 experiment consisted of three phases with constant level of total ionic strength of solutions (2
183 mM). Before bioreduction, transport experiments with the KCl input solution containing Br^- (85
184 mg/L KBr), DFBA (50 mg/L), and SSSNP (40 μg/L) were performed in all columns (phase 1).
185 In bioreduction process (phase 2), the columns were flushed with artificial groundwater solution
186 (AGW), which had a total ionic strength of 2 mM and a pH value of 7.5, consisting of $CaCl_2$
187 (0.075 mM), $MgCl_2$ (0.082 mM), KCl (0.051 mM), and $NaHCO_3$ (1.5 mM), modified from
188 Ferris et al. (2004). The AGW contained trace elements, vitamins, and acetate (bioreduction-

189 stimulated column) or without acetate (control column) (Wolin et al., 1963). Acetate added to the
190 columns served as the electron donor for *Geobacter*. Effluent samples from columns during
191 bioreduction were analyzed for the concentrations of Fe(II), Fe(III) and colloids as described in
192 Section 2.5. After 20 or 60 days of bioreduction, the same transport experiment as that prior to
193 bioreduction was performed (phase 3). Breakthrough and elution data for Br^-, DFBA, and
194 SSSNP were collected during phases 1 and 3. At the conclusion of the above procedures, the
195 columns were sectioned in 5-cm intervals along the longitudinal flow path of the columns. The
196 distribution of *Geobacter* and readily deducible iron content in soil aggregates from each section
197 were investigated as described in Section 2.7 and 2.8.

198 The third set of experiments was conducted to examine the effects of aggregate size
199 fractions on the transport of tracers and nanoparticles outside the anoxic chamber without
200 bioreduction treatment (exposed to oxygen), since exposure to aerobic conditions can suppress
201 reduction of iron oxides. The experiments included two columns, which were dry packed with
202 microaggregates and macroaggregates, respectively. The experimental procedures were the same
203 as those used in the second set of column experiments.

204 *2.5 Chemical analysis*

205 Bromide concentrations in the effluent fractions were determined using ion chromatography
206 as described elsewhere (Qin et al., 2017). The concentration of DFBA was measured with a
207 modified HPLC method (Galdiga and Greibrokk, 1998). Briefly, DFBA was resolved from other
208 effluent constituents using an Econosphere C-18 RP column (5 μm, 150 mm x 4.6 mm) with
209 isocratic elution using a mobile phase consisting of 95% K-phosphate buffer (5 mM, pH 3) and
210 5% acetonitrile (v/v) at a flow rate of 1.0 mL min^{-1}. DFBA was quantified using UV absorption

211 at 200 nm and the concentration was calculated via linear regression of peak area of external
212 DFBA standard solutions over a concentration range from 1 to 50 mg L^{-1}. All samples were
213 diluted 1:10 (v/v) in mobile phase to minimize sample matrix effects and filtered through 0.1 μm
214 membrane filters (Merck Millipore Ltd., Cork, Ireland) prior to analysis. SSSNP (with
215 hydrodynamic diameter of 129.8 nm) in effluent fractions were quantified by measuring the
216 concentration of silver by graphite furnace atomic absorption spectrometry using a Perkin-Elmer
217 Graphite Furnance AA equipped with a transversely heated graphite atomizer as described by
218 Fernández et al. (2010). Effluent samples were diluted 10^4 times with deionized water before
219 analysis, and 20 μL of diluted sample was injected with 10 μL of matrix modifier (prepared by
220 dissolving 0.05 mg de Pd and 0.003 mg $Mg(NO_3)_2$ in 10 μL 1% HNO_3). The silver detection
221 program in furnance AA was described in Fernández et al. (2010).

222 *2.6 Numerical modeling*

223 The HYDRUS code (Šimůnek et al., 2008) simulating saturated water flow based on the
224 Richards equation was used to simulate the transport of bromide, DFBA, and SSSNP. Transport
225 behaviors of Br^- and 2,6-DFBA were simulated using the classical advection-dispersion equation
226 (ADE). The transport and retention of SSSNP were simulated using the ADE with first-order
227 terms for kinetic retention and release as described in the HYDRUS code. The equation is given
228 in modeling the transport behavior as:

229 $$\frac{\partial(\theta C)}{\partial t} + \rho K_d \frac{\partial C}{\partial t} = \frac{\partial}{\partial z}\left(\theta D \frac{\partial C}{\partial z}\right) - \frac{\partial qC}{\partial z} - \theta \mu C$$

230 where θ[L^3L^{-3}] is the pore volume in the column, C [M L^{-3}; M represents the units of mass] is
231 the concentration of bromide, DFBA, and SSSNP in the aqueous phase, ρ [M L^{-3}] is the bulk
232 density of soil aggregates, K_d [L^3 M^{-1}] is the adsorption coefficient to soil aggregates, t is time

[T, T represents time units], D [$L^2 T^{-1}$] is the hydrodynamic dispersion coefficient, z [L] is the distance from the inlet of a column, q [$L T^{-1}$] is the Darcy velocity of input solutions, and μ [T^{-1}] is the first-order retention coefficient for tracer transformation processes.

2.7 Assessment of soil aggregate properties

Component analysis of soil aggregates were performed by commercial service of Midwest Laboratories Inc. (Omaha, NE, USA). Particle size distribution of soil aggregates was analyzed to indicate the reactivity behaviors of soil aggregates. The procedures and principles were described in Kemper and Rosenau (1986). Fifty grams of air-dried soil aggregates were presoaked in distilled water for 30 min and sieved with a top-down sequence of seven sieves of 2,000, 840, 300, 250, 150, 90, and 53 mm mesh size. The sieves with the contents were oscillated vertically in water with an amplitude of 4 cm at a rate of one oscillation per second for twenty times. The retained aggregates on each sieve after wet-sieving were recovered and dried at 50 °C in a drying oven. The particle size distribution was calculated with dry weight fractions. After bioreduction, dispersion of the aggregates was assessed based on readily reducible iron content. Soil aggregates from each section were homogenized, and 5-g sub-samples were placed in 50-mL centrifuge tubes, in which soil aggregates were shaken vigorously with 40-mL distilled water in an ice-water bath for 30 min (Kemper and Rosenau, 1986; Viollier et al., 2000). The mixtures were centrifuged at 4,248 g for 20 min, and the readily reducible iron in supernatant were determined using a modified Ferrozine method (Stookey, 1970). During column bioreduction experiments, the concentrations of Fe(II) and Fe(III) in the effluent were measured using a modified Ferrozine method (Stookey, 1970). Colloids were determined by centrifuging the effluent sample at 4,248 g for 20 min and measuring the mass of pellets after oven-drying, assuming the mass of dissolved salts was negligible.

2.8 DNA extraction and sequencing

To analyze the distribution of *Geobacter* in soil aggregates, DNA was extracted from fractioned soil aggregates using PowerLyser PowerSoil DNA isolation kit (MoBio Laboratories Inv. Carlsbad, California, USA). The DNA samples were quantified using PicoGreen Assay Kit (Carlsbad, CA, USA) and sent out for sequencing at HudsonAlpha Genomics Services Lab (Huntsville, AL, USA). The V3-V4 region of 16S rRNA gene of bacteria were amplified with primers of 341F_CCTACG GGNGGCWGCAG and 785R_GACTACHVGGGTATCTAATCC) in PCR. Finally, sequencing was performed using 300PE (paired-end) on the Illumina MiSeq platform (Illumina, USA). All methods were performed according to the manufacturers' protocol. Sequences analyses were performed using MOTHUR per standard operating procedure (Kozich et al., 2013). The results of these sequence analyses were used to calculate the relative abundance of *Geobacter* along the flow path in the columns.

3 Results and discussion

3.1 Effect of iron oxide on transport

The uncoated and goethite-coated quartz sands were used as simple and stable porous systems to evaluate the effect of iron oxide on the transport of tracers and nanoparticles. Br^- was included in the input solution to quantify transport behaviors of a diffusible tracer and to evaluate uniformity and integrity of the column packing in terms of hydrodynamic dispersion. As a conservative tracer, Br^- showed ideal and complete transport behavior in the sand with and without goethite coating (Fig. 1). In comparison, the breakthrough of SSSNP from the uncoated sand was slightly retarded relative to that of Br^- and eventually reached a stable maximum relative concentration (max C/C_0) of 0.85. However, almost no SSSNP broke through the

278 goethite-coated sand column. The fitted parameters of the breakthrough curves of SSSNP
279 showed a 14-fold increase in attachment and a 3-fold decrease in detachment of SSSNP in
280 goethite-coated sand compared with the uncoated sand columns. The maximum solid phase
281 concentration of SSSNP was ~20 times higher in the goethite-coated sand than in the uncoated
282 sand, suggesting a strong affinity of the SSSNP to the iron-oxide surface (Table 1). The strong
283 attachment of SSSNP to goethite-coated sand in this study was consistent with previous results
284 showing sequestration of silver nanoparticle (no silica-shell) by iron oxides (Sagee et al., 2012;
285 Liang et al., 2013).

286 *3.2 Effect of aggregates on transport*

287 To further determine if the change in soil aggregate sizes primarily influences the transport of
288 DFBA and SSSNP in column experiments, transport experiments were conducted in columns
289 packed with water-stable macroaggregates (250-2,000 μm) and microaggregates (53-250 μm)
290 under oxic conditions and without any reduction of Fe(III) oxides. The transport of bromide
291 through both aggregate fractions showed no obvious differences (Fig. 2); however, DFBA was
292 retarded in both columns, with larger retardation in the microaggregates (K_d of 0.12) than in the
293 macroaggregates (K_d of 0.06). Since the surface properties of macroaggregates and
294 microaggregates should have been very similar, the larger retardation is ascribed to the greater
295 total surface area and smaller pores of the microaggregates compared to the macroaggregates.
296 The breakthrough of SSSNP was negligible with both columns likely due to the strong
297 interactions of SSSNP with Fe(III) oxides (Fig. 2). Similar results of decreased silver
298 nanoparticle mobility in smaller soil aggregates were reported by Sagee et al. (2012), in which
299 the explanation was proposed that the reaction of silver nanoparticles with soil occurs at the
300 aggregate surface, and the smaller aggregates have increased surface area. Aggregate structure

has been shown to play an important role in retention of large molecules and nanoparticles with complicated interacting environmental factors (Sagee et al., 2012; Liang et al., 2013). For example, transport of silver nanoparticles in natural soil showed that aggregate size exerted major influence on silver nanoparticle transport, with silver nanoparticle mobility increased in the column of larger soil aggregates (Sagee et al., 2012). The transport and retention of silver nanoparticles in sand columns by Liang et al. (2013) also found that the mobility of silver nanoparticles was enhanced by increase in sand grain size. The soil aggregates used in this study were highly rich in iron oxides and had strong binding capacity for SSSNP, which caused complete retention of SSSNP in both microaggregates and macroaggregates columns. In contrast, the retardation of DFBA increased in the microaggregates.

3.3 Effect of short time bioreduction on transport

Soil aggregates rich in iron oxides were used to examine the effect of Fe(III)-bioreduction on transport behaviors of tracers and nanoparticles. The breakthrough of Br^- occurred at approximately one pore volume before and after the Fe(III)-bioreduction phase (Fig. 3), indicating that Fe(III)-bioreduction did not influence the transport of the conservative tracer. Transport of DFBA exhibited some retardation and tailing in the breakthrough experiment before the bioreduction, but the retardation was eliminated after the bioreduction phase (Figs. 3 and 4). This result suggests that Fe(III)-bioreduction induced either physical and/or chemical changes of the aggregates. Modeling results showed that the estimated dispersivity (D) of DFBA during transport remained similar before and after the Fe(III)-bioreduction phase while the estimated DFBA sorption coefficient (K_d) was about one order of magnitude lower after Fe(III)-bioreduction (Table 2). SSSNP exhibited a very pronounced response to the Fe(III)-bioreduction treatment. Almost no breakthrough of SSSNP was observed before Fe(III)-bioreduction (i.e., in

phase 1), whereas the relative concentrations (C/C_0) of SSSNP in the effluent reached only 0.3 after the Fe(III)-bioreduction (i.e., in phase 3) (Fig. 3). The estimated maximum solid phase concentration of SSSNP in phase 3 was one fourth that in phase 1 with a lower attachment coefficient. The estimated detachment coefficient of SSSNP was 100-fold greater in phase 3 than in phase 1 (Table 2). These results indicate that the presence of Fe(III) oxides greatly reduced the mobility of the nanoparticle tracer. Ryan et al. (1999) found that the bacteriophage particles and silica colloids attached to iron oxide-coated sand could be mobilized by anionic surfactant, elevated pH, and reductant, suggesting that iron oxide removal could promote the detachment of colloids and bacteriophage. Vink et al. (2017) showed that arsenic release corresponded to the fractions of readily reducible iron in sediments. At the initial phase of incubation with acetate-supplemented AGW solution, microbially mediated bioreduction released relatively small amount of Fe(II) from soil aggregates, causing certain alteration of the aggregate surface properties. Since the binding capacity for metals and colloids are highly dependent on ferric phases in soils (Pedersen et al., 2006), the reduction of iron oxides can lead to release of certain amount of retained molecules and colloids, such as DFBA and SSSNP.

The detection of soluble Fe(II) in the effluent indicated reduction of soil Fe(III) by *Geobacter* and/or other Fe(III)-reducing bacteria (Fig. 4). The increase in effluent Fe(II) concentrations in the first two weeks corresponded to the increase in microbial activity as acetate was added to the feed solution (Fig. 4). The effluent Fe(II) concentrations plateaued after 20 days of acetate injection, suggesting retardation of Fe(III) bioreduction (Fig. 5). The accumulated amount of Fe(II) in the effluent was approximately 0.125 mmol or about 0.04% of the total iron in the column. No Fe(III) oxides or other colloids were detected in the effluent during the 20-day bioreduction treatment. Although only a very small fraction of total Fe(III) was reduced to

soluble Fe(II) (assuming there were no secondary precipitation of Fe(II) in the column), the influences of Fe(III) reduction on the transport of DFBA and SSSNP were significant. This effect is attributable to Fe(II) binding to Fe(III) solids and/or the reduction of the most bioavailable Fe(III) on the external surfaces of the aggregates and/or along the advective pathways that are most accessible by less diffusible microorganisms and particle tracers (e.g., SSSNP). Removal of surface iron oxides during bioreduction could reduce positive electric charges and roughness on mineral surfaces (Joe-Wong et al., 2017), causing a decrease in surface deposition of nanoparticles.

An in-situ study investigating the mobility of arsenate in natural groundwater showed that arsenic desorption occurred with reductive dissolution of ferric oxides in ferrihydrite, goethite, and hematite (Zhang et al., 2017). Microbial metabolism can affect the affinity of nanoparticles, and therefore cause the simultaneous releases of Fe and Fe(III)- oxide-bound particles. Similarly, Moon et al. (2017) reported that the genus *Geobacter*, *Anaeromyxobacter*, and *Desulfosporosinus* might play important roles in release of arsenic coupled with iron reduction. In this study, the concentration of Fe(II) in the effluent increased with time during the 20-day treatment demonstrating bioreduction of iron oxides in the acetate-treated soil column. However, without Fe(III) oxides or other colloids detected in the effluent, no evidence of structural breakdown in soil aggregates was observed during the whole bioreduction process. The enhanced transport of SSSNP was most likely attributed to the microbial reduction-induced transformation of iron minerals, resulting in less contact of SSSNP with iron oxides. A very recent study by Xiao et al. (2018) reported that the transformation from less crystalline to more crystalline iron oxides by iron reducing bacterium *Shewanella oneidensis* MR-1 affected the

behavior of any species absorbed to the iron oxides, suggesting that the produced Fe(II) can stimulate the reduction and transformation of iron oxide minerals.

3.4 Effect of long time bioreduction on transport

Given only 0.04% of the total iron was detected in the effluent in the 20-day bioreduction experiment, additional aggregate-packed column experiments with the duration of acetate-stimulated Fe(III)-bioreduction extended to 60 days were conducted to further examine the effect of bioreduction on Fe(II) release, aggregate breakdown, and tracer transport. The transport behaviors of bromide and DFBA showed no change after the 60-day Fe(III)-bioreduction treatment, whereas SSSNP were completely retained in the soil aggregates both before and after the 60-day acetate injection (Fig. 6 and Table 2). These results are inconsistent with the observations made in the short time experiment with 20-day acetate injection, where Fe(III)-bioreduction resulted in earlier breakthrough of DFBA and SSSNP. The longer duration of Fe(III)-bioreduction (60 d) brought about as yet unknown changes to the properties of soil aggregates and resulted in complete retention of the SSSNP particles, though retardation and slow release of the DFBA were not observed in the short time experiment.

The release of soluble Fe(II) in the 60-day experiment was similar to the 20-day experiments during the first 20 days but exhibited a steady increase in the effluent Fe(II) concentration through day 60 (Fig. 7). The concentration of soluble Fe(II) reached 300 μM, or more than 10 times the total amount observed at the end of the 20-day Fe(III) bioreduction experiment. The accumulated amount of soluble Fe(II) collected in the effluent was 1.43 mmol or about 0.48% of the total Fe in the soil aggregates within the column. Colloids were first detected in the effluent at 30 days after the acetate injection and continued to increase in concentration during the 60-day

391 Fe(III)-bioreduction treatment, further suggesting that Fe(III)-bioreduction and aggregate
392 breakdown were active throughout the biostimulation phase of the soil column experiment (Fig.
393 7). A small amount of Fe(II) was also detected in the effluent of the control column, indicating
394 that *Geobacter* was able to couple oxidation of the native soil organic carbon with Fe(III)
395 reduction. The inconsistent tracer transport results between the 20-day and 60-day bioreduction
396 experiments very likely arose from the greater aggregate breakdown that occurred during the
397 extended period (day 20-60) than the initial period (day 0-20) of the bioreduction treatment. The
398 aggregate breakdown generated soil colloids, which may have increased mechanical straining of
399 SSSNP in soil pores and may have exposed aggregate interior Fe(III)-oxide surfaces promoting
400 the attachment of SSSNP on positively charged surfaces.

401 *3.5 Effect of long time bioreduction on aggregate structure*

402 The above results suggested that the soil aggregates experienced structural breakdown during
403 the 60-day Fe(III)-bioreduction phase with acetate injection. To get direct evidence, we
404 characterized the size distribution of water-stable soil aggregates in each column. The acetate-
405 treated columns contained significantly more soil aggregates with size less than 90 μm than the
406 control column (i.e., no acetate injection) ($P < 0.05$, Fig. 8). The aggregate fractions with sizes
407 of 150-2,000 μm in acetate-treated columns were similar to those in the control column. It is
408 obvious that the soil aggregates enduring 60-day bioreduction generated more microaggregates
409 compared to the soil aggregates with 20-day bioreduction.

410 Our results also show that the bioreduction increased releases of iron and soil colloids. The
411 divergence of soil aggregates along the length of the columns was also examined by measuring
412 residual water-extractable total Fe. The readily reducible iron contained in the soil aggregates
413 was much higher in the influent sections of the 60-day acetate-fed columns (A and B) with a

range of 20-25 mg g^{-1} compared to the control (Fig. 9). The readily reducible iron in the effluent sections of the acetate-fed columns was less than 5 mg g^{-1}. In the control column, the water-extractable iron content ranged between 4.5 and 5.5 mg g^{-1} in the influent sections to less than 1 mg g^{-1} in the effluent section. The amounts of readily reducible iron in the acetate-amended columns exceeded that of the control column by approximately five fold. These trends were very consistent with the distribution of the relative abundance of *Geobacter* in the columns (Fig. 9), suggesting that Fe(III)-bioreduction by *Geobacter* contributed to the releases of iron and colloids. These results indicate more significant structural breakdown of the soil aggregates in the soil depths receiving more electron donors.

4. Conclusions and implications

Acetate injection stimulated microbially mediated Fe(III)-oxide reduction, and when delivered for a relatively short duration (i.e. 20 d) it enhanced the transport of an organic molecular tracer (DFBA) and nanoparticle tracers (silica-shelled silver nanoparticles) compared with the transport exhibited prior to acetate injection. However, in the subsequent experiment, when the acetate injection period was extended to 60 d the impact on transport disappeared and the transport of all tracers was identical in acetate treated and control columns despite significant aggregate structural breakdown in the acetate treated columns. The limited data suggest that soil aggregates had minimal structural breakdown during the first 20-day of bioreduction, and as a result, only Fe(III)-oxides coating the exterior surfaces of the aggregates were reduced, yielding advective flow paths with chemically less reactive surfaces that were unfavorable for the attachment of organic and colloidal tracers on the aggregates. In comparison, more aggregates were dispersed during the 60-day bioreduction experiment, causing exposure of interior Fe(III)-oxide surfaces, generating larger reactive surfaces that were favorable for the attachment of

437 organic and colloidal tracers. As a result, the initial 20-day effect was canceled by the subsequent
438 40-day of extended acetate injection, leading to similar breakthrough behaviors to those observed
439 before the Fe(III)-bioreduction phase. Electron donor addition during biostimulation cannot
440 continue indefinitely. Thus, upon termination of biostimulation, the treated area will ultimately
441 return to its original redox status as oxygenated groundwater passes through the treatment zone.
442 Future studies should address the influence of Fe(II) re-oxidation on tracer transport in relation to
443 changes in soil properties, such as, pore structure and aggregate surface charges along the flow
444 path.

445 **Conflict of Interest**

446 The authors declare no conflicts of interest.

447 **Acknowledgments**

448 The authors acknowledge with tremendous respect, the contributions of Dr. Phillip Jardine
449 (posthumously) and his collaborators (Drs. Colleen Hansel, Jack Parker, Ungtae Kim, and Kirk
450 Scheckel) for conceiving and executing the research upon which the current work was founded.
451 This research was financially supported by the Strategic Environmental Research and
452 Development Program (SERDP) under project ER-2130. We also acknowledge financial support
453 from the China Scholarship Council to support X.L.

454

455

456

457

458 **References**

459 Arora, B., Mohanty, B.P., McGuire, J.T., 2015. An integrated Markov chain Monte Carlo
460 algorithm for upscaling hydrological and geochemical parameters from column to field
461 scale. Sci. Total Environ. 512, 428-443. https://doi.org/10.1016/j.scitotenv.2015.01.048.

462 Aulenta, F., Majone, M., Tandoi, V., 2006. Enhanced anaerobic bioremediation of chlorinated
463 solvents: environmental factors influencing microbial activity and their relevance under field
464 conditions. J. Chem. Technol. Biotechnol. 81, 1463-1474. https://doi.org/10.1002/jctb.1567.

465 Bose, P., Sharma, A., 2002. Role of iron in controlling speciation and mobilization of arsenic in
466 subsurface environment. Water Res. 36, 4916–4926. https://doi.org/10.1016/S0043-
467 1354(02)00203-8.

468 Bradford, S.A., Torkzaban, S., 2008. Colloid transport and retention in unsaturated porous
469 media: a review of interface-, collector-, and pore-scale processes and models. Vadose Zone
470 J. 7, 667-681. https://doi.org/10.2136/vzj2007.0092.

471 Braunschweig, J., Bosch, J., Meckenstock, R.U., 2013. Iron oxide nanoparticles in
472 geomicrobiology: from biogeochemistry to bioremediation. New Biotechnol. 30, 793-802.
473 https://doi.org/10.1016/j.nbt.2013.03.008.

474 Caccavo, F., Lonergan, D.J., Lovley, D.R., Davis, M., Stolz, J.F., McInerney, M.J., 1994.
475 *Geobacter sulfurreducens* sp. Nov., a hydrogen- and acetate-oxidizing dissimilatory metal-
476 reducing microorganism. Appl. Environ. Microbiol. 60, 3752-3759.

477 Caldwell, M.E., Tanner, R.S, Suflita, J.M, 1999. Microbial metabolism of benzene and the
478 oxidation of ferrous iron under anaerobic conditions: implications for bioremediation.
479 Environ. Microbiol. 5, 595-565. https://doi.org/10.1006/anae.1999.0193.

480 Chapelle, F.H., Lovley, D.R., 1992. Competitive exclusion of sulfate reduction by Fe(lll)-
481 reducing bacteria: a mechanism for producing discrete zones of high-iron ground water.
482 Ground Water 30, 29-36. https://doi.org/10.1111/j.1745-6584.1992.tb00808.x.

483 Coates, J.D., Anderson, R.T., 2000. Emerging techniques for anaerobic bioremediation of
484 contaminated environments. Trends Biotechnol. 18, 408-412. https://doi.org/10.1016/S0167-
485 7799(00)01478-5

486 De-Camposa, A.B, Mamedovb, A.I., Huang, C.H., 2009. Short-term reducing conditions
487 decrease soil aggregation. Soil Sci. Soc. Am. J. 73, 550-559.
488 https://doi.org/10.2136/sssaj2007.0425.

489 Deng, L., Yuan, P., Liu, D., Annabi-Bergaya, F., Zhou, J., Chen, F., Liu, Z., 2017. Effects of
490 microstructure of clay minerals, montmorillonite, kaolinite and halloysite, on their benzene
491 adsorption behaviors. Appl. Clay Sci. 143, 184-191.
492 https://doi.org/10.1016/j.clay.2017.03.035.

493 Ellis, D.E., Lutz, E.J., Odom, J.M., Buchanan, R.J., Bartlett, C.L., Lee, M.D., Harkness, M.R.,
494 DeWeerd, K.A., 2000. Bioaugmentation for accelerated in situ anaerobic bioremediation.
495 Environ. Sci. Technol. 34, 2254–2260. https://doi.org/10.1021/es990638e.

496 Fernández, A., Picouet, P., Lloret, E., 2010. Cellulose-silver nanoparticle hybrid materials to
497 control spoilage-related microflora in absorbent pads located in trays of fresh-cut melon. Int.
498 J. Food Microbiol. 142, 222-228. https://doi.org/10.1016/j.ijfoodmicro.2010.07.001.

499 Ferris, F.G., Phoenix, V., Fujita, Y., Smith, R.W., 2004. Kinetics of calcite precipitation induced
500 by ureolytic bacteria at 10 to 20 C in artificial groundwater. Geochim. Cosmochim. Acta 68,
501 1701-1710. https://doi.org/10.1016/S0016-7037(03)00503-9.

502 Galdiga, C.U., Greibrokk, T., 1998. Trace analysis of fluorinated aromatic carboxylic acids in
503 aqueous reservoir fluids by HPLC. J. Liq. Chromatogr. Relat. Technol. 21, 855-868.
504 https://doi.org/10.1080/10826079808000514.

505 Goldberg, S., Kapoor, B.S., Rhoades, J.D., 1990. Effect of aluminum and iron oxides and
506 organic matter on flocculation and dispersion of arid zone soils. Soil Sci. 150, 588-593.

507 Guan, Z., Tang, X.Y., Nishimura, T., Katou, H., Liu, H.Y., Qing, J., 2017. Surfactant-enhanced
508 flushing enhances colloid transport and alters macroporosity in diesel-contaminated soil. J.
509 Environ. Sci. http://dx.doi.org/10.1016/j.jes.2017.06.006.

510 Hansel, C.M., Benner, S.G., Neiss, J., Dohnalkova, A., Kukkadapu, R.K, Fendorf, S., 2003.
511 Secondary mineralization pathways induced by dissimilatory iron reduction of ferrihydrite
512 under advective flow. Geochim. Cosmochim. Acta 67, 2977–2992.
513 http://dx.doi.org/10.1016/S0016-7037(03)00276-X.

514 Hansel, C.M., Benner, S.G., Fendorf, S., 2005. Competing Fe(II)-induced mineralization
515 pathways of ferrihydrite. Environ. Sci. Technol. 39, 7147-7153.
516 http://dx.doi.org/10.1021/es050666z.

517 Joe-Wong, C., Brown Jr, G.E., Maher, K., 2017. Kinetics and Products of Chromium (VI)
518 Reduction by Iron (II/III)-Bearing Clay Minerals. Environ. Sci. Technol. 51, 9817-9825.
519 https://doi.org/10.1021/acs.est.7b02934.

520 Karadimitriou, N.K., Joekar-Niasar, V., Brizuela, O.G., 2017. Hydro-dynamic Solute Transport
521 under Two-Phase Flow Conditions. Sci. Rep. 7, 6624. http://dx.doi.org/10.1038/s41598-
522 017-06748-1.

523 Kemper W.D., Rosenau R.C., 1986. Aggregate stabilty and size distribution. In: Klute A, ed.
524 Methods of soil analysis, Part 2 chemical and mineralogical methods (2nd edition).
525 Madison: Soil Science Society of America. Fitchburg, WI, pp. 491-515

526 Kozich, J.J., Westcott, S.L., Baxter, N.T., Highlander, S.K., Schloss, P.D., 2013. Development of
527 a dual-index sequencing strategy and curation pipeline for analyzing amplicon sequence data
528 on the MiSeq Illumina sequencing platform. Appl. Environ. Microbiol. 79, 5112-5120.
529 http://dx.doi.org/10.1128/AEM.01043-13.

530 Jardine, P.M., 2008. Influence of coupled processes on contaminant fate and transport in
531 subsurface environments. Adv. Agron. 99, 1-99. https://doi.org/10.1016/S0065-
532 2113(08)00401-X.

533 Liang, X., Shi, R., Radosevich, M., Zhao, F., Zhang, Y., Han, S., Zhang, Y., 2017. Anaerobic
534 lipopeptide biosurfactant production by an engineered bacterial strain for in situ microbial
535 enhanced oil recovery. RSC Adv. 7, 20667-20676. https://doi.org/10.1039/C7RA02453C.

536 Liang, Y., Bradford, S.A., Simunek, J., Vereecken, H., Klumpp, E., 2013. Sensitivity of the
537 transport and retention of stabilized silver nanoparticles to physicochemical factors. Water
538 Res. 47, 2572-2582. https://doi.org/10.1016/j.watres.2013.02.025.

539 Loffler, F.E., Sanford, R.A., Tiedje, J.M., 1996. Initial Characterization of a Reductive
540 Dehalogenase from Desulfitobacterium chlororespirans Co23. Appl. Environ. Microbiol. 62,
541 3809-3813.

542 Lovley, D.R., 2003. Cleaning up with genomics: applying molecular biology to bioremediation.
543 Nat. Rev. Microbiol. 1, 35-44. https://doi.org/10.1038/nrmicro731.

544 Maurice, P.A., Hochella, M.F., 2008. Nanoscale particles and processes: a new dimension in soil
545 science. Adv. Agron. 100, 123-153. https://doi.org/10.1016/S0065-2113(08)00605-6.

546 Mayes, M.A., Jardine, P.M., Mehlhorn, T.L., Bjornstad, B.N., Ladd, J.L., Zachara, J.M., 2003.
547 Hydrologic processes controlling the transport of contaminants in humid region structured
548 soils and semi-arid laminated sediments. J. Hydrol. 275, 141-161.
549 https://doi.org/10.1016/S0022-1694(03)00039-8.

550 McCarthy, J.F., McKay, L.D., 2004. Colloid transport in the subsurface: past, present and future
551 challenges. Vadose Zone J. 3, 326-337. https://doi.org/10.2136/vzj2004.0326.

552 McKay, L.D., Sanford, W.E., Strong, J.M., 2000. Field-scale migration of colloidal tracers in a
553 fractured shale saprolite. Ground Water 38, 139-147. https://doi.org/10.1111/j.1745-
554 6584.2000.tb00211.x.

555 Mehra, O.P., Jackson, M.L, 1960. Iron oxide removal from soils and clays by dithionite-citrate
556 system buffered with sodium bicarbonate. Clay. Clay Miner. 7, 317-327.
557 https://doi.org/10.1016/B978-0-08-009235-5.50026-7.

558 Mejia, J., Roden, E.E., Ginder-Vogel, M., 2016. Influence of oxygen and nitrate on Fe (hydr)
559 oxide mineral transformation and soil microbial communities during redox cycling. Environ.
560 Sci. Technol. 50, 3580-3588. https://doi.org/10.1021/acs.est.5b05519.

561 Mohanty, S.K., Saiers, J.E., Ryan, J.N., 2016. Colloid mobilization in a fractured soil: effect of
562 pore-water exchange between preferential flow paths and soil matrix. Environ. Sci. Technol.
563 50, 2310-2317. https://doi.org/10.1021/acs.est.5b04767.

564 Moon, H.S., Kim, B.A., Hyun, S.P., Lee, Y.H., Shin, D., 2017. Effect of the redox dynamics on
565 microbial-mediated As transformation coupled with Fe and S in flow-through sediment
566 columns. J. Hazard. Mater. 329, 280-289. https://doi.org/10.1016/j.jhazmat.2017.01.034.

567 Pachapur, V.L., Larios, A.D., Cledon, M., Brar, S.K., Verma, M., Surampalli, R.Y., 2016.
568 Behavior and characterization of titanium dioxide and silver nanoparticles in soils. Sci. Total
569 Environ. 563, 933-943. https://doi.org/10.1016/j.scitotenv.2015.11.090.

570 Pedersen, H.D., Postma, D., Jakobsen, R., 2006. Release of arsenic associated with the reduction
571 and transformation of iron oxides. Geochim. Cosmochim. Acta 70, 4116–4129.
572 https://doi.org/10.1016/j.gca.2006.06.1370.

573 Qin, Q., Chen, X.J., Zhuang, J., 2017. The surface-pore integrated effect of soil organic matter
574 on retention and transport of pharmaceuticals and personal care products in soils. Sci. Total
575 Environ. 599, 42-49. https://doi.org/10.1016/j.scitotenv.2017.04.148.

576 Ryan, J.N., Elimelech, M., Ard, R.A., Harvey, R.W., Johnson, P.R., 1999. Bacteriophage PRD1
577 and silica colloid transport and recovery in an iron oxide-coated sand aquifer. Environ. Sci.
578 Technol. 33, 63-73. https://doi.org/10.1021/es980350.

579 Sagee, O., Dror, I., Berkowitz, B., 2012. Transport of silver nanoparticles (AgNPs) in soil.
580 Chemosphere 88, 670-675. https://doi.org/10.1016/j.chemosphere.2012.03.055.

581 Schaider, L.A., Senn, D.B., Estes, E.R., Brabander, D.J., Shine, J.P., 2014. Sources and fates of
582 heavy metals in a mining-impacted stream: temporal variability and the role of iron oxides.
583 Sci. Total Environ. 490, 456-466. https://doi.org/10.1016/j.scitotenv.2014.04.126.

584 Si, Y., Zou, Y., Liu, X., Si, X., Mao, J., 2015. Mercury methylation coupled to iron reduction by
585 dissimilatory iron-reducing bacteria. Chemosphere 122, 206-212.
586 https://doi.org/10.1016/j.chemosphere.2014.11.054.

587 Šimůnek, J., van Genuchten, M.T. and Šejna, M., 2008. Development and applications of the
588 HYDRUS and STANMOD software packages and related codes. Vadose Zone J. 7,
589 https://doi.org/587-600.10.2136/vzj2007.0077.

590 Song, B., Zeng, G., Gong, J., Liang, J., Xu, P., Liu, Z., Zhang, Y., Zhang, C., Cheng, M., Liu, Y.,
591 Ye, S., 2017. Evaluation methods for assessing effectiveness of in situ remediation of soil
592 and sediment contaminated with organic pollutants and heavy metals. Environ. Int. 105, 43-
593 55. https://doi.org/10.1016/j.envint.2017.05.001.

594 Stookey, L.L., 1970. Ferrozine—a new spectrophotometric reagent for iron. Anal. Chem. 42,
595 779-781. https://doi.org/10.1021/ac60289a016.

596 Thompson, A., Chadwick, O.A., Boman, S., Chorover, J., 2006. Colloid mobilization during soil
597 iron redox oscillations. Environ. Sci. Technol. 40, 5743–5749.
598 https://doi.org/10.1021/es061203b.

599 Vink, J.P., van Zomeren, A., Dijkstra, J.J., Comans, R.N., 2017. When soils become sediments:
600 Large-scale storage of soils in sandpits and lakes and the impact of reduction kinetics on
601 heavy metals and arsenic release to groundwater. Environ. Pollut. 227, 146-156.
602 https://doi.org/10.1016/j.envpol.2017.04.016.

603 Viollier, E., Inglett, P.W., Hunter, K., Roychoudhury, A.N., van Cappellen, P., 2000. The
604 ferrozine method revisited: Fe(II)/Fe(III) determination in natural waters. Appl. Geochem.
605 15, 785-790. https://doi.org/10.1016/S0883-2927(99)00097-9.

606 Weber, K.A., Achenbach, L.A., Coates, J.D., 2006. Microorganisms pumping iron: anaerobic
607 microbial iron oxidation and reduction. Nat. Rev. Microbiol. 4, 752-764.
608 https://doi.org/10.1038/nrmicro1490.

609 Wolin, F.A., Wolin, M.J., Wolfe, R.S., 1963. Formation of methane by bacterial extracts. J. Biol.
610 Chem. 238, 2882-2886.

611 Xiao, W., Jones, A.M., Li, X., Collins, R.N., Waite, T.D., 2018. Effect of Shewanella oneidensis
612 on the kinetics of Fe (II)-catalyzed transformation of ferrihydrite to crystalline iron oxides.
613 Environ. Sci. Technol. 52, 114-123. https://doi.org/10.1021/acs.est.7b05098.

614 Zhang, D., Guo, H., Xiu, W., Ni, P., Zheng, H., Wei, C., 2017. In-situ mobilization and
615 transformation of iron oxides-adsorbed arsenate in natural groundwater. J. Hazard. Mater.
616 321, 228-237. https://doi.org/10.1016/j.jhazmat.2016.09.021.

617 Zhuang, J., Jin, Y., Flury, M., 2003. Colloid-facilitated cesium transport through water-saturated
618 Hanford sediment and Ottawa sand. Environ. Sci. Technol. 37, 4905-4911.
619 https://doi.org/10.1021/es0264504.

620 Zhuang, J., Qi, J., Jin, Y., 2005. Retention and transport of amphiphilic colloids under
621 unsaturated flow conditions: effect of particle size and surface properties. Environ. Sci.
622 Technol. 39, 7853-7859. https://doi.org/10.1021/es050265j.

623 Zhuang, J., McCarthy, J.F., Perfect E., Tyner, J., Flury, M., 2007. In-situ colloid mobilization in
624 Hanford sediments under unsaturated transient flow condition: Effect of irrigation pattern.
625 Environ. Sci. Technol. 41, 3199-3204. https://doi.org/10.1021/es062757h.

626 Zhuang, J., Jin, Y., 2008. Interactions between virus and goethite during saturated flow: effects
627 of solution pH, carbonate, and phosphate. J. Contam. Hydrol. 98, 15-21.
628 https://doi.org/10.1016/j.jconhyd.2008.02.002.

629 Zhuang, J., Tyner, J.S., Perfect, E., 2009. Colloid transport and remobilization in unsaturated
630 porous media during transient flow. J. Hydrol. 377, 112-119.
631 https://doi.org/10.1016/j.jhydrol.2009.08.011.

632 Zhuang, J., Goeppert, N., Tu, C., McCarthy, J.F., Perfect, E., McKay, L.D., 2010. Colloid
633 transport with wetting fronts: Interactive effects of solution surface tension and ionic
634 strength. Water Res. 44, 1270-1278. https://doi.org/10.1016/j.watres.2009.12.012.

635

636 **Table 1.** Model fitted parameters for silica-shelled silver nanaparticle breakthrough from columns

Silica-shelled silver nanoparticle	Sand	Geothite-coated sand
Maximum solid phase concentration (N_c M^{-1})	0.560	12.000
Attachment coefficient (min^{-1})	0.007	0.100
Detachment coefficient (min^{-1})	0.001	0.0003

637
638
639
640
641
642
643
644
645

Table 2. Model fitted parameters for 2,6-DFBA and SSSNP breakthrough from water-stable soil aggregate columns before (Pre-) and after (Post-) Fe(III)-bioreduction.

Tracer	Parameter	[§]Fe(III)-bioreduction phase (20 d)		Fe(III)-bioreduction phase (60 d)					
				Column A		Column B		Column C	
Tracer	Parameter	[#]Pre	*Post	Pre	Post	Pre	Post	Pre	Post
2,6-DFBA	*D* (cm)	1.12	0.93	0.89	0.84	0.85	0.82	0.84	0.83
	K_d (cm^3mg^{-1})	0.086	0.0063	0.014	0.011	0.041	0.031	0.027	0.001
	S_{max}	23.6	5.55	[ϕ] -	-	-	-	-	-
SSSNP	Att. Coeff. (min^{-1})	0.046	0.026	-	-	-	-	-	-
	Detach Coeff. (min^{-1})	$3x10^{-6}$	$7.7x10^{-4}$	-	-	-	-	-	-

[§]Data were collected from a single column.

[#]Tracer transport experiment before stimulation of Fe(III)-bioreduction by injection of acetate.

*Tracer transport experiment after stimulation of Fe(III)-bioreduction by injection of acetate.

[ϕ]Breakthrough of SSSNP colloids was not detected in either the treated or control columns.

D is dispersivity.

K_d is sorption coefficient.

S_{max} [N_c M^{-1}] is the maximum solid phase concentration of SSSNP.

646

647

648

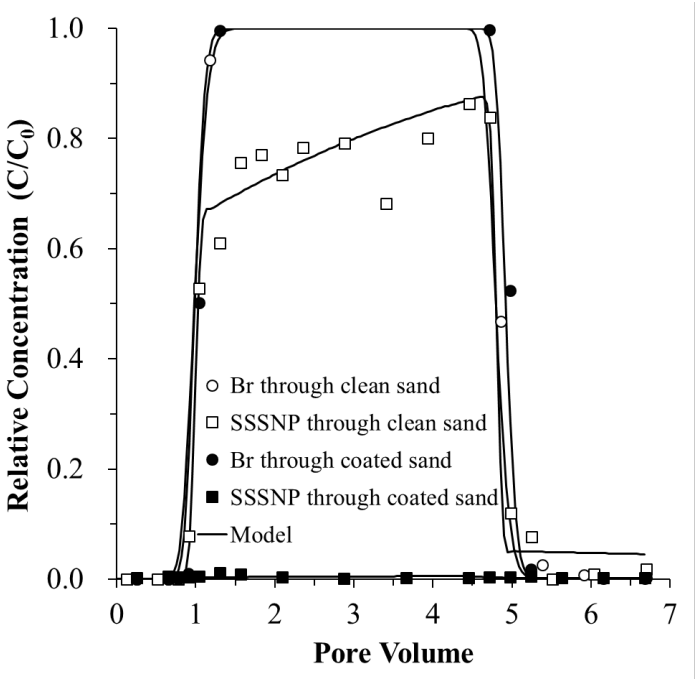

649

650 **Fig. 1.** Transport of bromide and silica-shelled silver nanoparticles (SSSNP) through goethite-
651 coated and uncoated sands. The concentrations of bromide and SSSNP are shown over pore
652 volume with columns flushed using KCl solution (0.67 mM, pH 6.5).

653

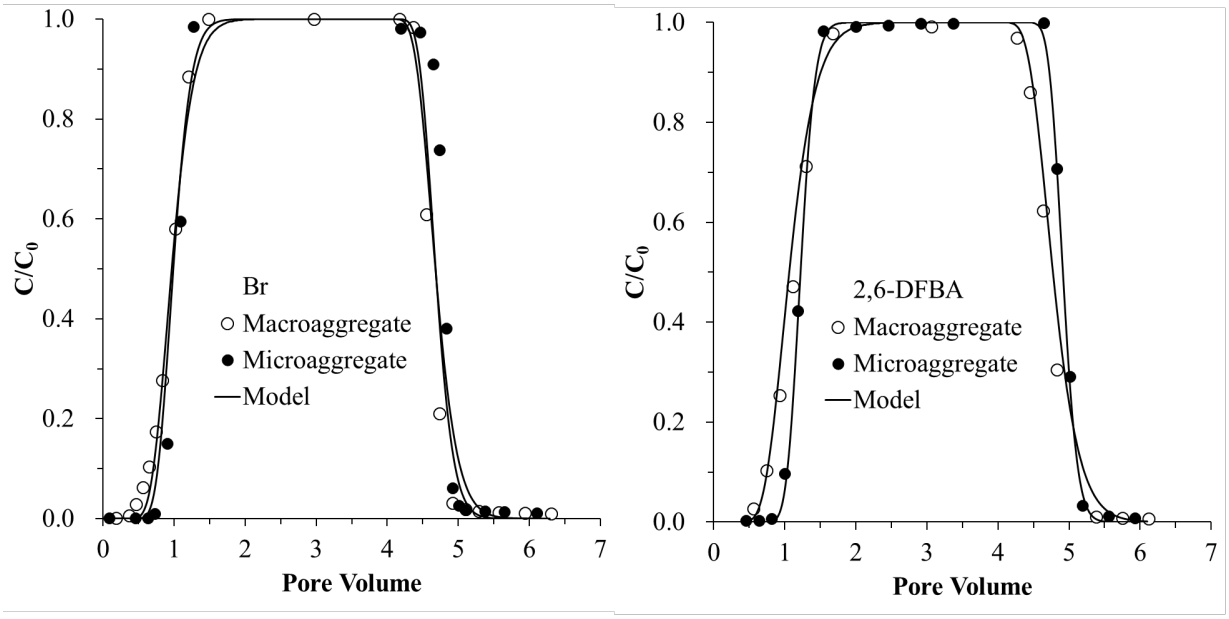

Fig. 2. Transport of bromide and DFBA through columns packed with water-stable macroaggregaes (250-2,000 μm) or water-stable microaggregates (53-250 μm) under oxic conditions without Fe(III)-bioreduction.

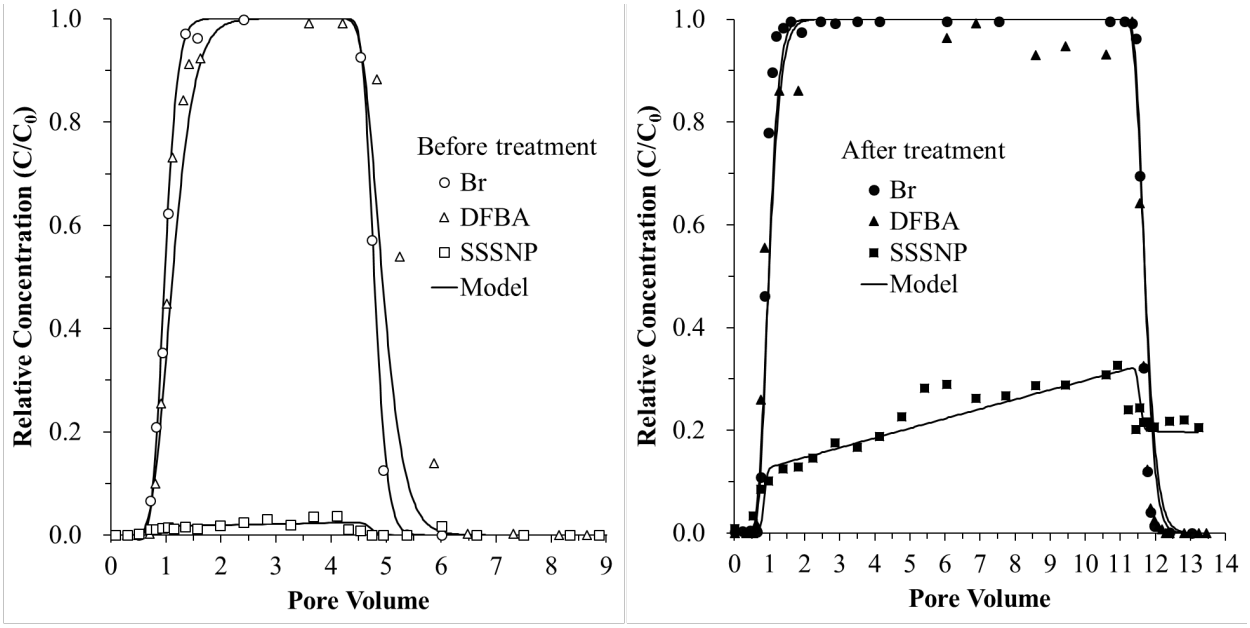

Fig. 3. Breakthrough curves of tracers (Br^- and DFBA) and silica-shelled silver nanoparticles (SSSNP) from columns packed with water-stable soil aggregates before and after the 20-day Fe(III)-bioreduction.

667

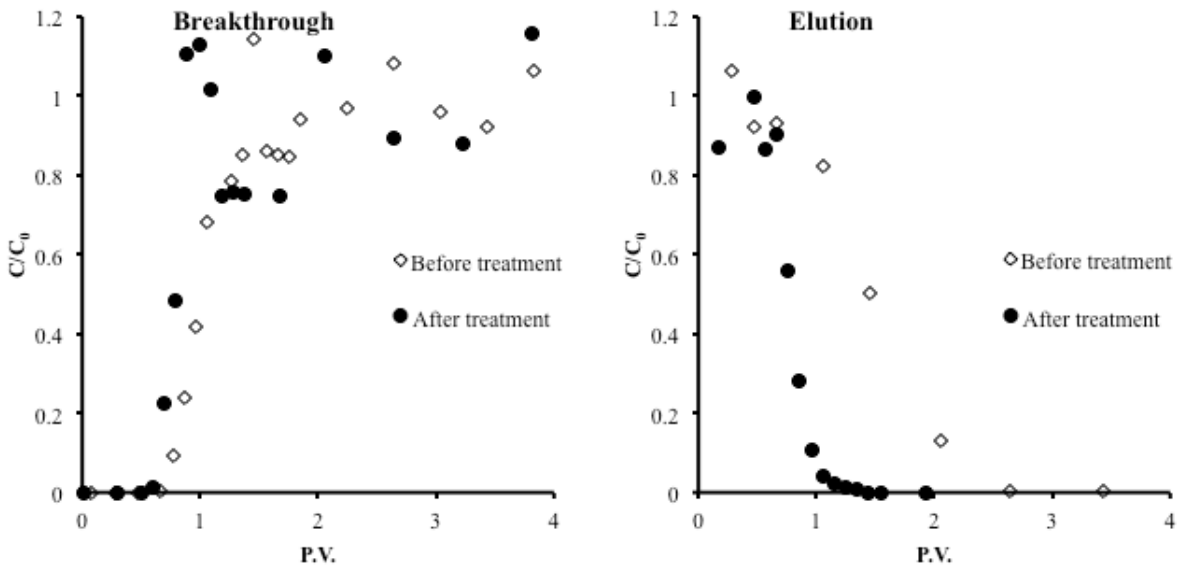

Fig. 4. Expanded view of breakthrough and elution profiles of DFBA before and after the 20-day Fe(III)-bioreduction phase.

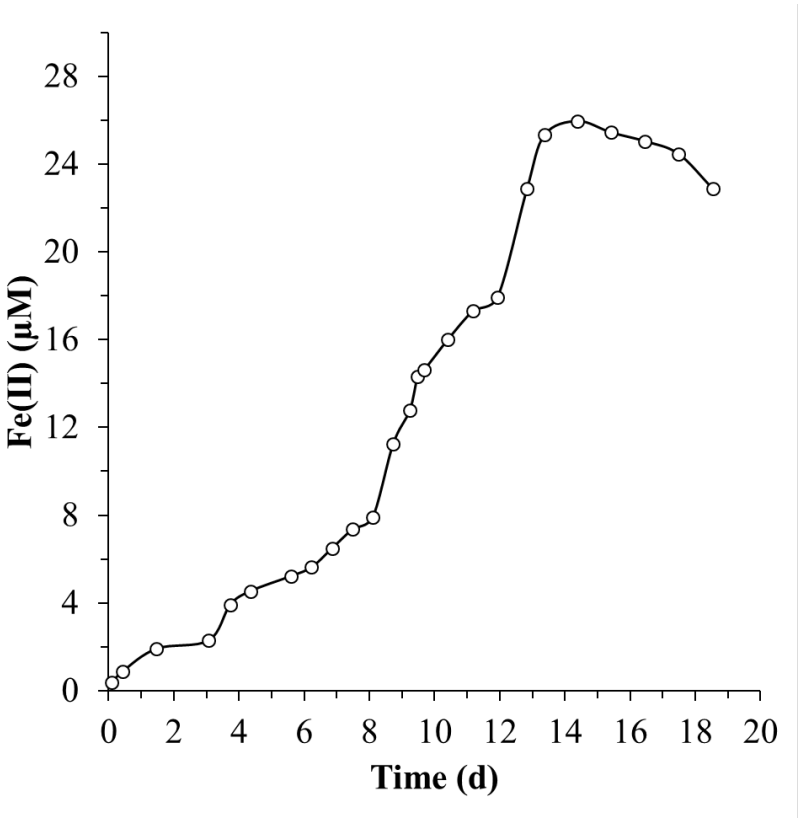

668

669 **Fig. 5.** Effluent Fe(II) concentration during the acetate injection phase of the 20-day Fe(III)-
670 bioreduction column experiment.

671

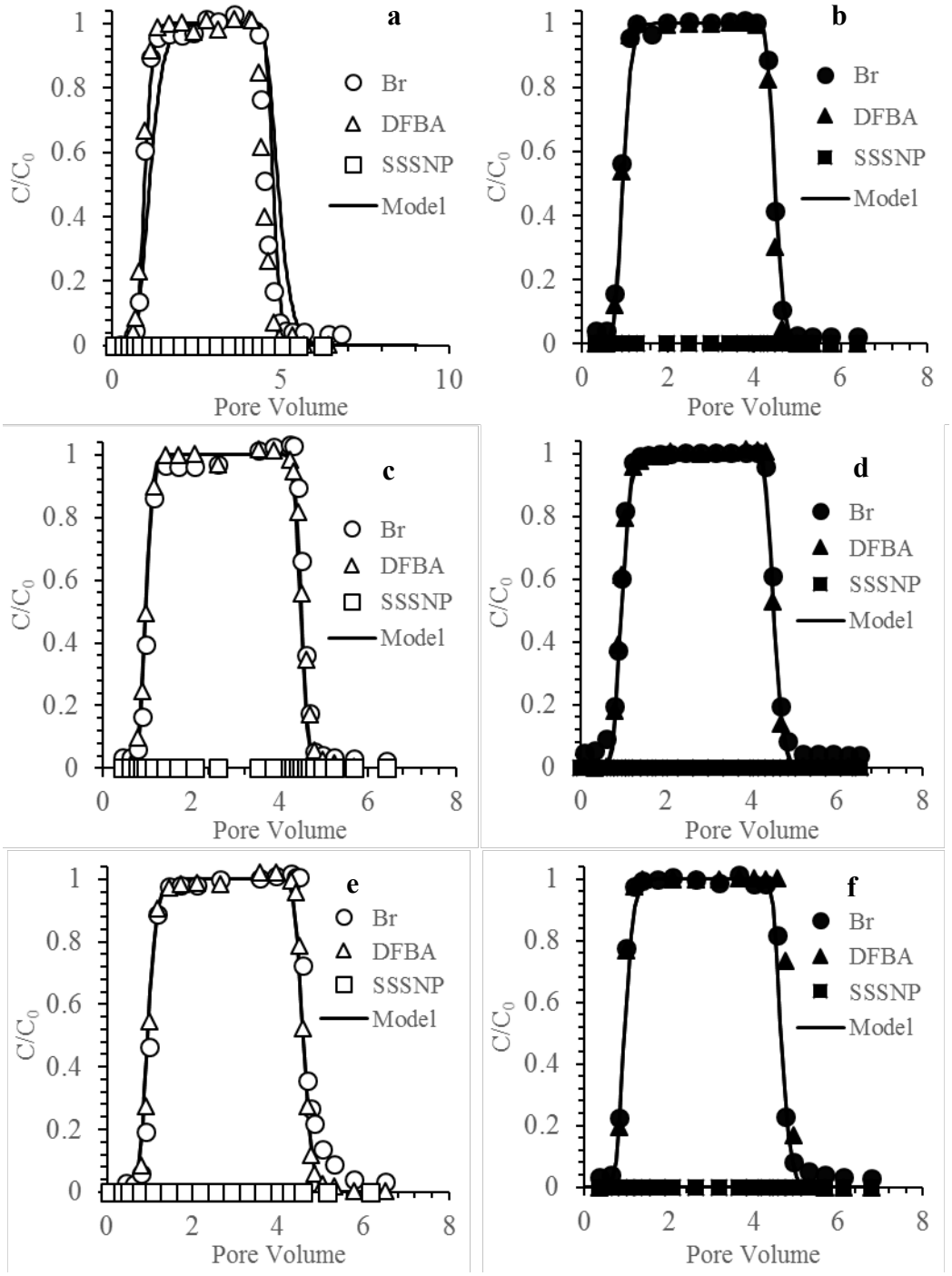

Fig. 6. Breakthrough curves of tracers (Br^- and DFBA) and silica-shelled silver nanoparticles (SSSNP) in pre- (left, a, c, e) and post-acetate (right, b, d, f) treatment transport experiments for 60-day Fe(III)-bioreduction treatment in the columns packed with water-stable macroaggregates (250-2,000 µm). The plots of a, b, c, and d are breakthrough curves from replicate acetate-treated columns while the plots of e and f are breakthrough curves from the control column that did not receive acetate injection.

679

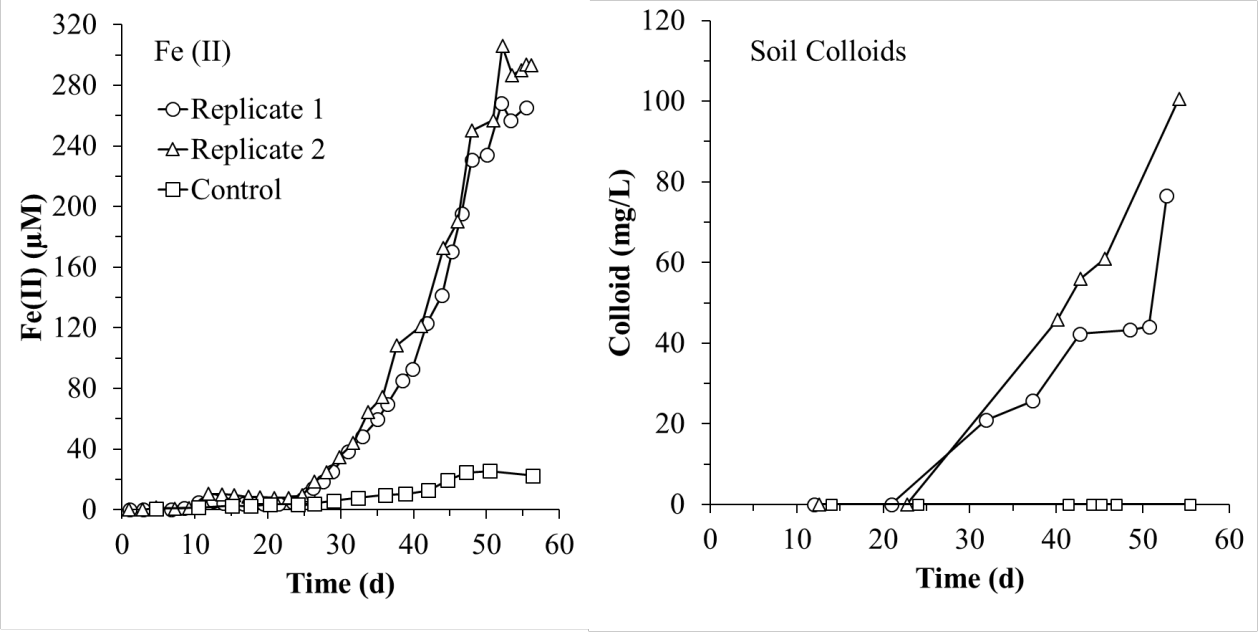

680 **Fig. 7.** Concentrations of released Fe(II) and soil colloids in the effluent during the acetate
681 injection phase of the 60-day Fe(III)-bioreduction column experiments.

682

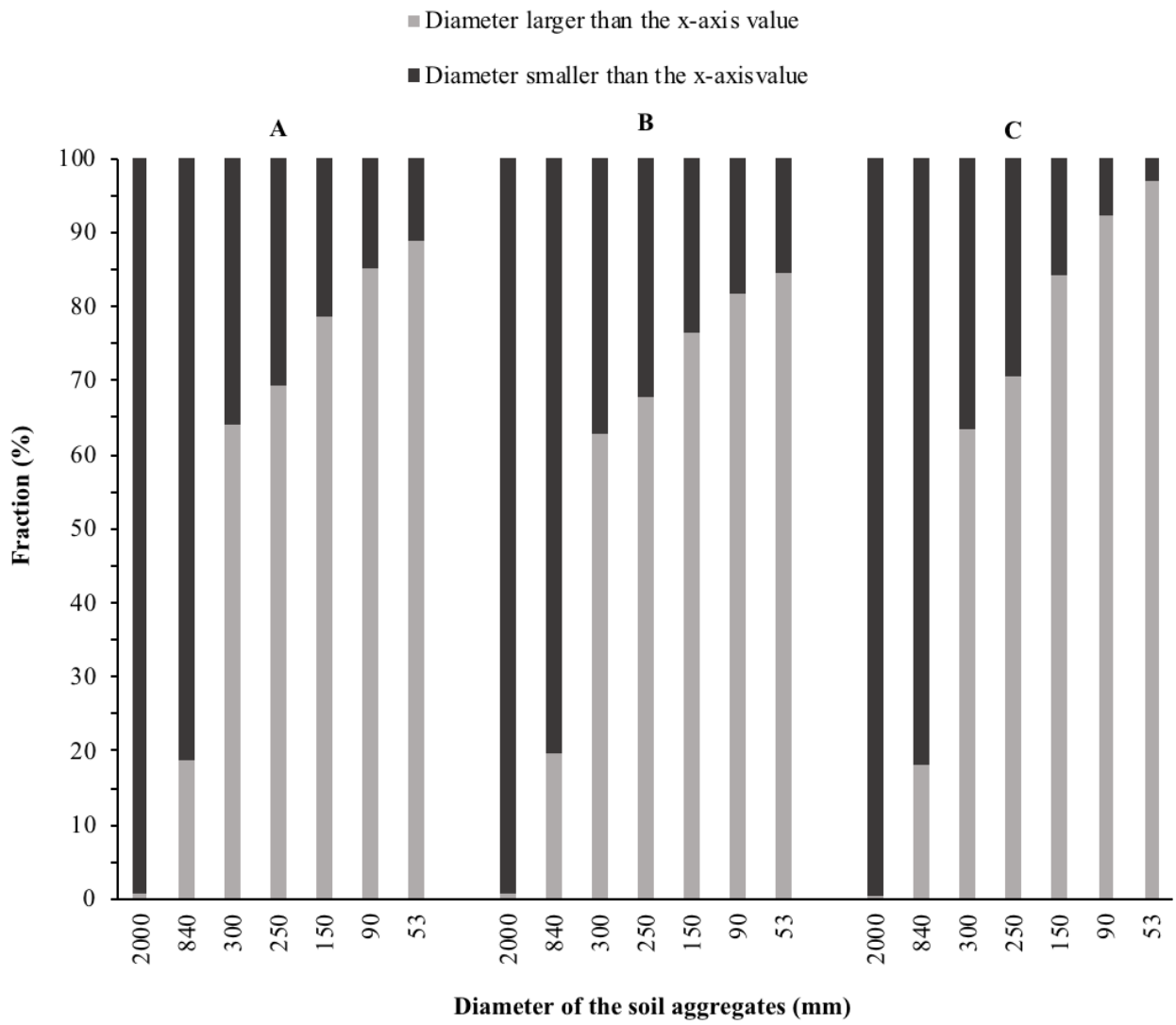

683
684

685 **Fig. 8.** The aggregate size distribution of the soil aggregates from the aggregate-packed columns
686 after the conclusion of the 60-day Fe(III)-bioreduction experiment. Columns A and B received
687 acetate in the feed solution over a 60-day period. Column C was the control column without
688 acetate injection.

689

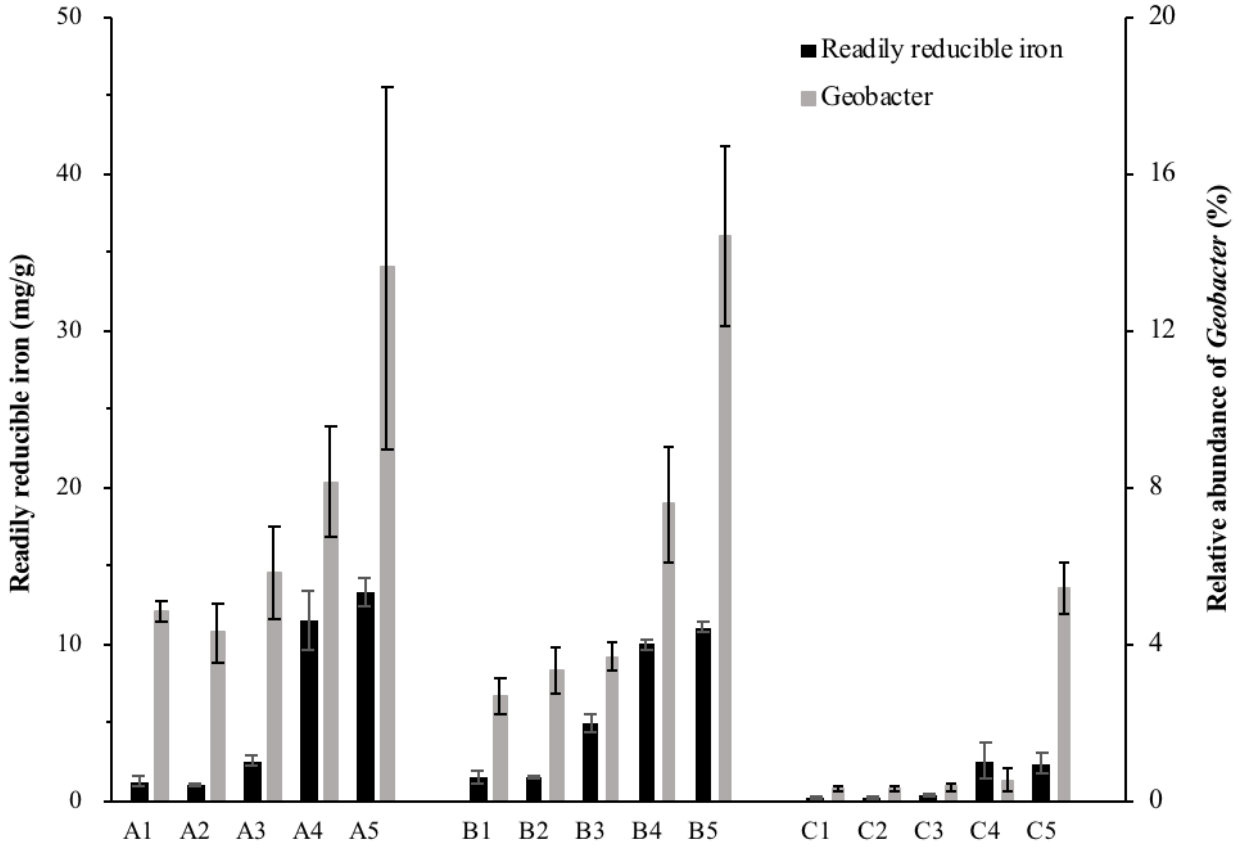

690

691 **Fig. 9.** Readily reducible iron content and distribution of iron-reducing bacteria (*Geobacter*
692 determined via sequencing of 16S rRNA gene libraries prepared from soil samples) in five
693 depths of the aggregate-packed columns at the conclusion of the 60-day Fe(III)-bioreduction
694 column experiment. Columns A and B received acetate in the feed solution over a 60-day period.
695 Column C, the control column, did not receive any acetate. Sections 1 and 5 represent samples
696 collected near the effluent and influent ends of the columns, respectively.

697

698 **Supplementary Materials**

699

700 **Table S1.** Experimental protocols of transport tests in columns.

Transport experiments	Columns No.	Porous media	Procedures
Investigation of effects of iron oxide on the transport of tracers and nanoparticles	1	Goethite-coated silica	1. Two columns were wet-packed with uncoated and goethite-coated sands, respectively. 2. The sand columns were flushed with KCl solution (0.67 mM, pH 6.5) prior to the tracer experiments. 3. The input solution for the sand columns contained Br- (50 mg/L KBr), DFBA (40 mg/L), and SSSNP (40 ug/L) in the KCl solution. 4. Breakthrough and elution data of three tracers were collected.
	2	Uncoated silica	
Evaluations of the effect of Fe(III)-bioreduction on the transport of tracers (bioreduction duration of 20 days and 60 days, seperately)	3	Macroaggregates (250-2000 µm)	1. Five columns were dry-packed with *Geobactor*-inoculated soil macroaggregates under anoxic conditions. 2. The soil aggregate columns were flushed with carbon dioxide to replace the air in soil pores, followed by flushing with KCl solution (0.67 mM, pH 6.5) to achieve fully saturated conditions without remaining gas pockets. 3. Each column experiment consisted of three phases with constant total ionic strength of solutions (2 mM): **Phase 1:** Tracer transport experiments with the KCl input solution containing Br- (85 mg/L KBr), DPBA (50 mg/L), and SSSNP (40 µg/L).Breakthrough and elution data of three tracers were collected. **Phase 2:** Columns were flushed with artificial groundwater solution (AGW), which had a total ionic strength of 2 mM and a pH value of 7.5, consisting of CaCl2 (0.075 mM), MgCl2 (0.082 mM), KCl (0.051 mM), NaHCO3 (1.5 mM), trace elements, and vitamins. The AGW for bioreduction-stimulated column contained acetate, while the AGW for two control columns was prepared without acetate. The bioreducgtion phase lasted for 20 days in two columns (acetate-treated column 3 and control column 4); while the other three columns (acetate-treated columns A and B, and control column C) experienced 60 days of bioreduction. **Phase 3:** The same tracer transport experiments with Phase 1 were performed at the conclusion of bioreduction phase.
	4	Macroaggregates (250-2000 µm)	
	A	Macroaggregates (250-2000 µm)	
	B	Macroaggregates (250-2000 µm)	
	C	Macroaggregates (250-2000 µm)	

Examinations of the effects of aggregate size fractions on the transport of three tracers	5	Macroaggregates (250-2000 µm)	1. Two columns were dry packed with microaggregates and macroaggregates, respectively. 2. The soil aggregate columns were flushed with carbon dioxide, followed by flushing with KCl solution (0.67 mM, pH 6.5) to achieve fully saturated conditions without remaining gas pockets. 3. Tracer experiments withBr- (50 mg/L KBr), DFBA (40 mg/L), and SSSNP (40 ug/L) in the KCl solution were performed in each column. 4. Breakthrough and elution data of three tracers were collected.
	6	Microaggregates (53-250 µm)	

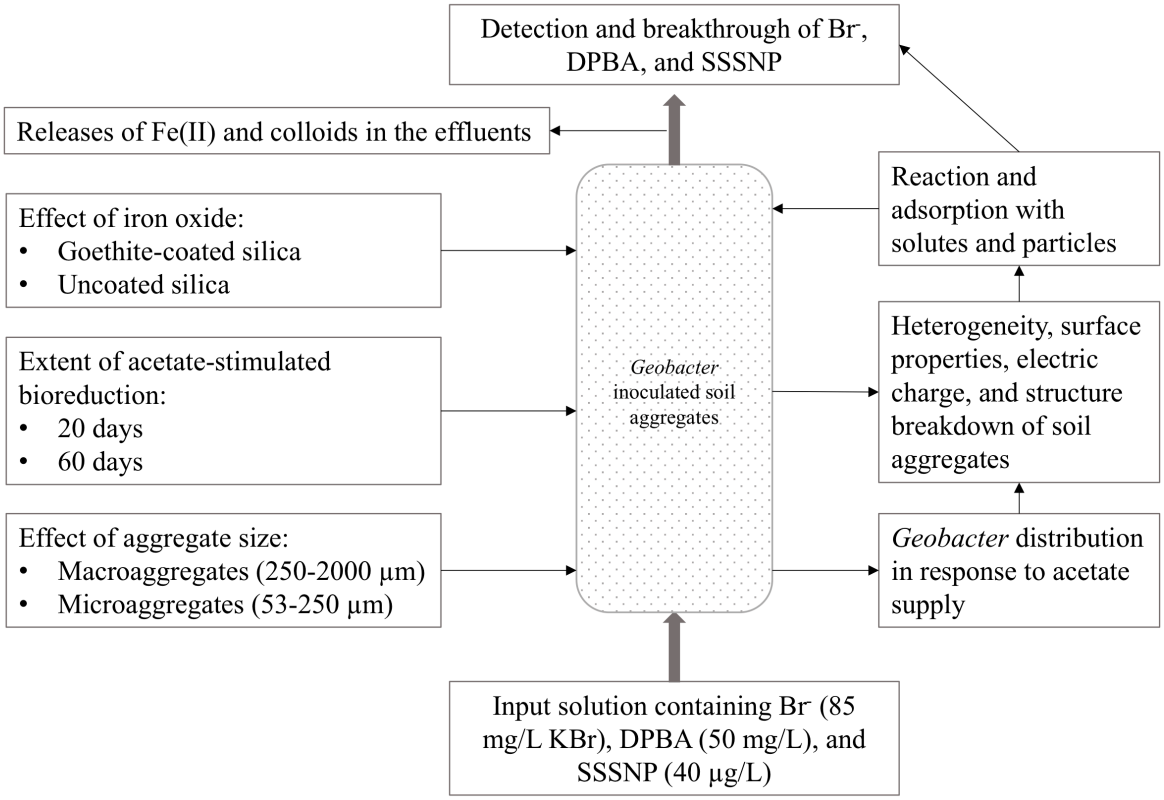

Fig. S1. The schematic diagram of column experiments.